NREL
NATIONAL RENEWABLE ENERGY LABORATORY

Model Fidelity Study of Dynamic Transient Loads in a Wind Turbine Gearbox

Preprint

Y. Guo and J. Keller
National Renewable Energy Laboratory

T. Moan and Y. Xing
Centre for Ships and Ocean Structures (CeSOS) - Norwegian University of Science and Technology (NTNU)

To be presented at the 2013 WINDPOWER Conference
Chicago, Illinois
May 5 – 8, 2013

Conference Paper
NREL/CP-5000-58414
April 2013

Contract No. DE-AC36-08GO28308

Model Fidelity Study of Dynamic Transient Loads in a Wind Turbine gearbox

Yihan Xing*	Yi Guo	Jonathan Keller	Torgeir Moan
CeSOS, NTNU	NWTC, NREL	NWTC, NREL	CeSOS, NTNU
Trondheim, Norway	Colorado, USA	Colorado, USA	Trondheim, Norway

Abstract

Transient events cause high loads in wind turbine drivetrain components, so measuring and calculating these loads can improve confidence in drivetrain design. This paper studies the response of the Gearbox Reliability Collaborative 750-kW wind turbine gearbox during transient events using a combined experimental and modelling approach. The transient events include emergency shutdowns and start-ups measured during a field testing period in 2009. The drivetrain model is established in the multibody simulation tool Simpack. A study of modelling fidelity required for accurate load prediction was performed and results were compared against measured loads. A high-fidelity model that includes shaft and housing flexibility and accurate bearing stiffnesses is important for the higher-speed stage bearing loads. Including the flexibility of main shaft and planet carrier is important to simulate shutdown events compared to start-ups because main shaft bending loads are much higher in shutdown events than those during startups.

Keywords: wind turbine gearbox, field-test measurements, multibody method, transient events

1. Introduction

The gearbox is a crucial and expensive component of the wind turbine and has experienced higher-than-expected failure rates. De Vries [1] suggested that there is a lack of insight in transient drivetrain behaviour that occurs during control actions or generator faults. These transients can lead to unexpected torque reversals and generator faults that can be harmful to drivetrain components. Understanding the effects of transient events on wind turbine gearboxes is important, and this paper examines the modelling of the gearbox under such events.

In previous work, the authors have performed various modelling studies of the National Renewable Energy Laboratory (NREL) Gearbox Reliability Collaborative's (GRC) gearbox [2]. This included the study of the required model fidelity with comparisons to dynamometer test measurements in LaCava el al. [3, 4] and detailed study of the modelling of the planet carrier in Xing et al. [5]. Other examples of work in gearbox modelling include LaCava et al. [6, 7], Oyague el al. [8-11], Peeters et al. [12-14], Helsen et al. [15-18], Xing et al. [19, 20] and Guo et al. [21, 22]. The results from the previous work have been positive, however, the validated drivetrain model for test stand conditions might not perform as well for field conditions. Furthermore, these previous works focused almost solely on measurements in the low-speed planetary stage. This paper takes the previous work a step further by using comparisons against actual field-test measurements and additional gearbox stages. The field-test measurements provide a unique opportunity to further validate the multibody drivetrain models against field conditions. It is also important to compare the models against transient field measurements as the original models that were validated using steady-state dynamometer tests might not work as well for the transient-load cases. The work performed in this paper fills this gap in model validation.

This work is presented in three parts. First, the multibody drivetrain model is compared against the measurements from two transient load events. The variables compared are the planet bearing radial forces during a normal start-up and an emergency shutdown. Second, a more detailed model fidelity study of the multibody drivetrain model involving response variables from all the stages is performed using the measurements as inputs. Finally, the effect of individual flexible bodies on the calculated responses is also investigated.

*yihan.xing@ntnu.no

2. Test Article

The test article used for this study was the wind turbine (WT) from the National Renewable Energy Laboratory's (NREL) Gearbox Reliability Collaborative (GRC) project [2]. The GRC WT is a 750-kW, stall-regulated, dual-speed, three-bladed upwind machine. The GRC gearbox has one planetary and two parallel stages and uses the three-point support system. The input and output shafts are not co-axial. Its topology is similar to those of the larger, conventional, variable-speed, multimegawatt gearboxes seen today. The GRC drivetrain and gearbox are shown in Figure 1. The steady-state system characteristics of the GRC WT are presented in Figure 2. The WT is parked above the cut-out wind speed of 25 m/s. The gearbox topology and naming convention for each individual bearing is presented in Figure 3. The INP-A (spherical roller bearing) represents the main shaft bearing; PLC-A and PLC-B (full complement cylindrical roller bearings) represent the planet carrier bearings; and PL-A and PL-B (cylindrical roller bearings) represent the planet gear bearings. LS-SH-A, LS-SH-B and LS-SH-C, IMS-SH-A, IMS-SH-B and IMS-SH-C and HS-SH-A, HS-SH-B and HS-SH-C represent the low-, intermediate-, and high-speed stage bearings, respectively. The upwind bearings in these stages are cylindrical roller bearings, while the downwind bearings are tapered roller bearings. The B and C bearings, therefore, carry the axial forces acting on the shafts in this bearing setup. A floating sun system should allow for better load sharing between the three planet gears in the low-speed planetary stage.

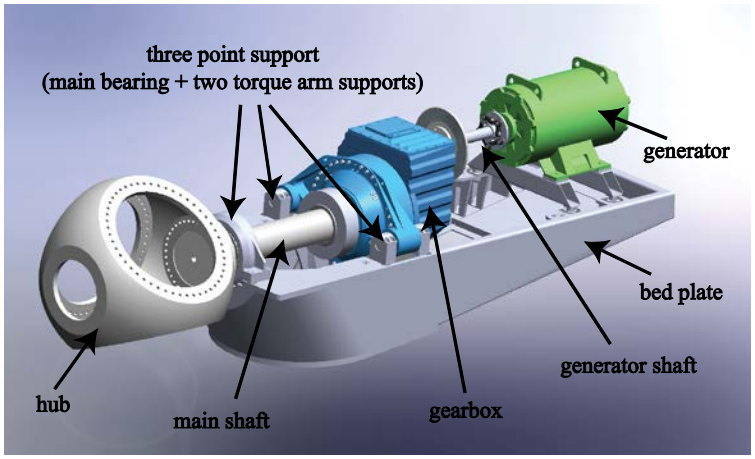

Figure 1: The GRC drivetrain and gearbox

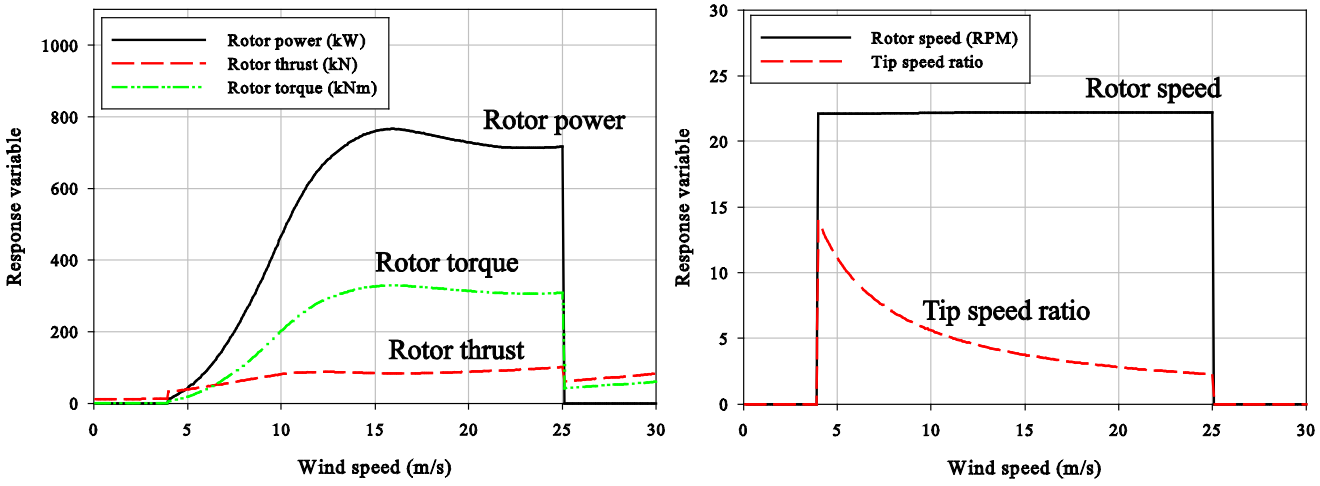

Figure 2: The GRC WT steady-state system characteristics calculated by FAST

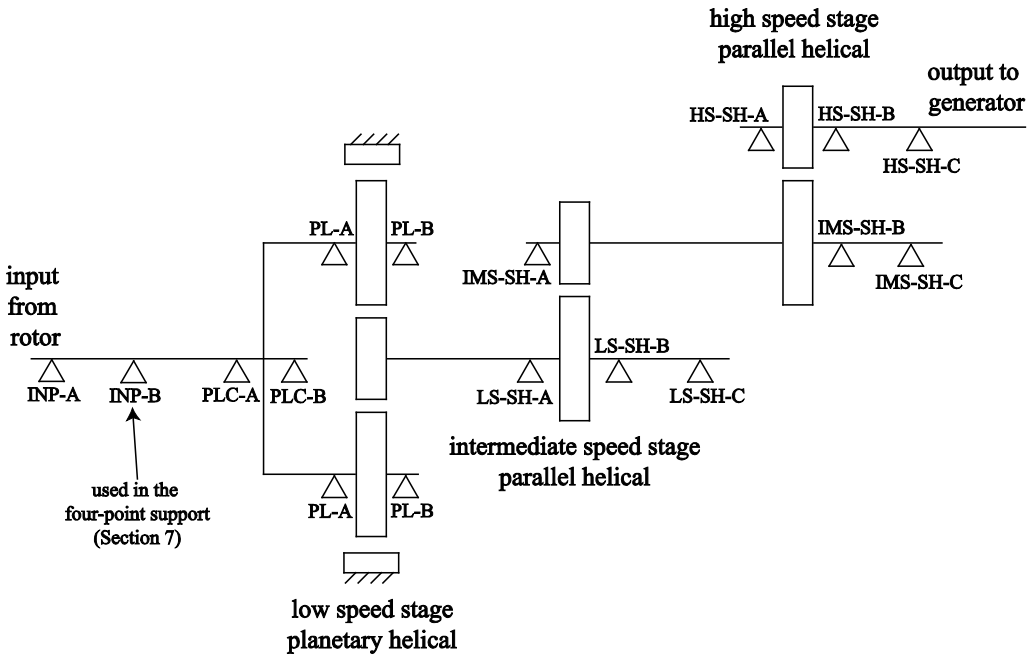

Figure 3: The GRC gearbox topology

2.1. Measurement Setup

The GRC project instrumented two gearboxes for dynamometer and field testing. Internal measurements include gear tooth loads, component deflections and misalignments, and planet bearing loads. The full description of instrumentation is detailed in Link et al. [2]. The instrumentation used to measure the planet bearing loads is shown in Figure 4. For each planet bearing, three axial slots were machined into the inner diameter of the inner ring and instrumented with strain and temperature gauges. Two of the slots were located at different circumferential locations in the bearing load zone for each planet, and the third slot for every bearing was oriented 90° from the sun-planet axis (referred to here as top dead center or TDC). Two gauge sets in each TDC slot and two bearings on each planet provided an axial distribution of four radial loads along each planet pin.

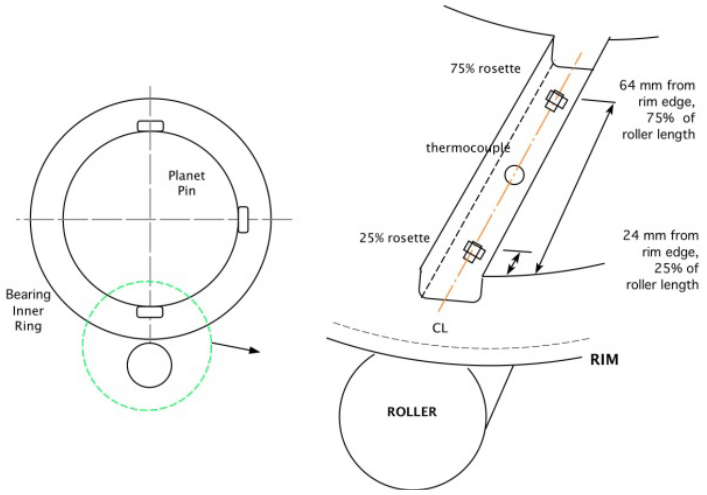

Figure 4: Strain gauges mounted on the planet bearing inner races from Link at al. [2]

3. Multibody Simulation of the Drivetrain

The drivetrain is modelled using the multipurpose multibody simulation software, SIMPACK. Each component of the drivetrain is modelled as a rigid or flexible body. The components are interconnected using joints, force elements, and constraints. The shafts, planet carrier, gearbox housing, and bedplate can be modelled as flexible bodies. The flexible bodies are modelled using condensed finite element (FE) models imported from Abaqus. These flexible bodies are derived via a two-step process. First, a condensation of the FE model is performed to yield reduced mass and stiffness matrices. Second, modal analysis is performed on the reduced matrices to yield the eigenmodes, and a subset of these modes is chosen for the final flexible body. This final flexible body is used in SIMPACK. In the planet carrier model, a total of nine interface nodes for the main shaft, pin interfaces, and the bearing interfaces are retained. These nodes are also coupled to their respective regions of nodes. A rigid coupling constraint for the main-shaft interface and flexible coupling constraints for the remaining interfaces are found to be ideal in Xing et al. [5]. The gear wheels are modelled using rigid bodies with tooth compliance. Tooth compliance is modelled using SIMPACK's gear pair element, FE225, which models gear contact as a series of discrete springs and dampers. The gear stiffness is calculated in accordance with ISO 6336-1 [23]. This stiffness parameter depends on the location of the contact point and the gear geometry. The forces and torques acting on each individual gear are then calculated as a function of the gear stiffness and the penetration depth at the gear teeth. The FE225 element also considers normal damping, coulomb friction, backlash, and micro-geometry. The bearings are modelled using force elements that use stiffness matrices to represent the bearing stiffness.

No one single model is perfect for all types of simulations; therefore, this paper will also study the level of model fidelity required to reproduce the various field-test measurements. The level of model fidelity depends on the load conditions imposed on the model and the level of detail expected in the results. In Xing et al. [5], only the planetary stage was modelled as the main focus was a very detailed model of the planet carrier. On the other hand, in the drivetrain study of a floating spar-type wind turbine [19, 20], a drivetrain model that consists of six DOF gearwheels, bearing compliances, and flexible shafts were found to be sufficient for reasonable accuracy in the statistical responses in the drivetrain. Therefore, this level of model fidelity was chosen for that work. Figure 5 shows the SIMPACK model topology for the entire drivetrain used in this paper. The application of the main-shaft loads and generator speed into the multibody drivetrain model is illustrated in Figure 6. The main-shaft loads and generator speed are obtained from the measurements in this paper.

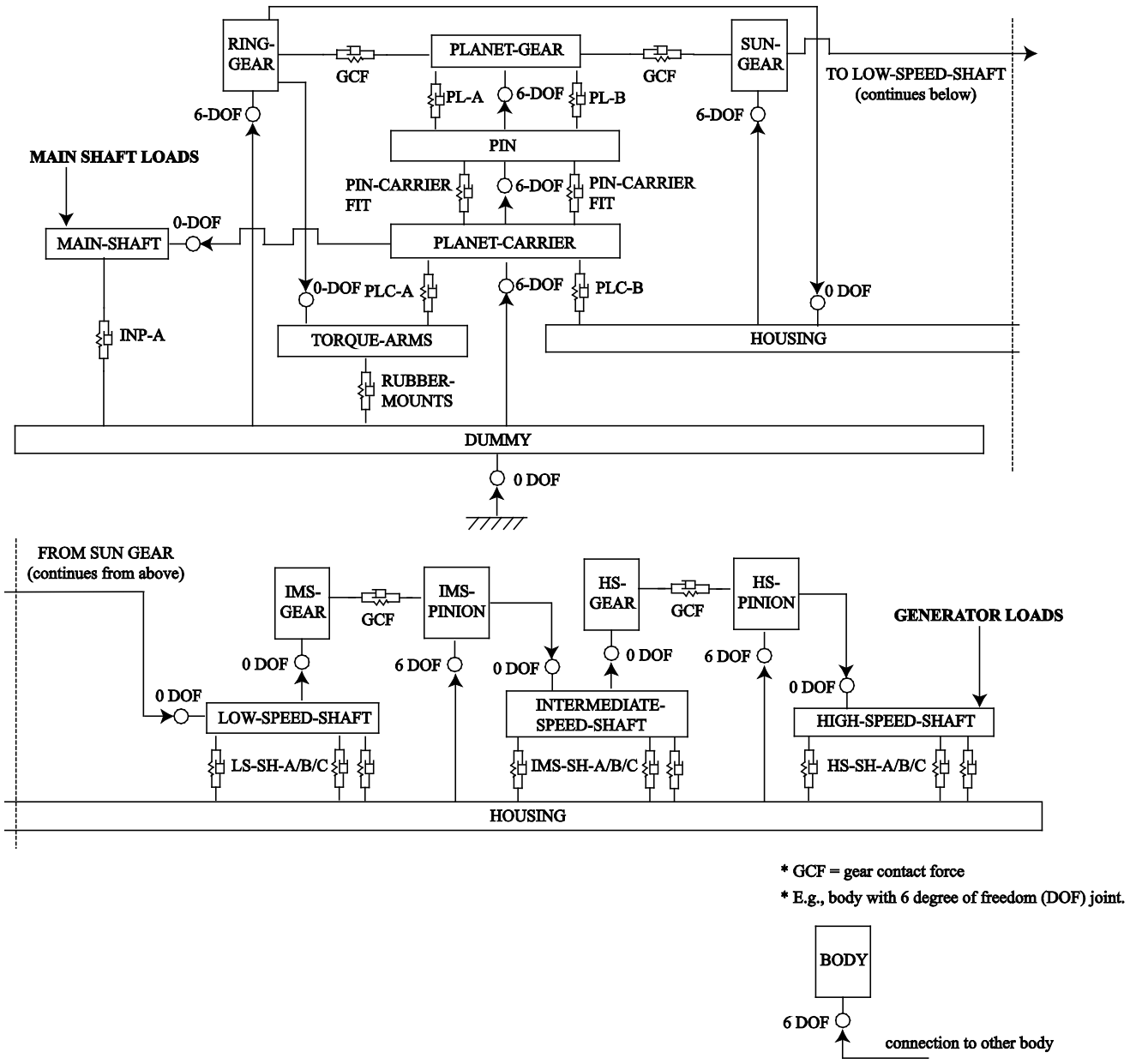

Figure 5: SIMPACK model topology of the entire drivetrain. DOF stands for degree of freedom.

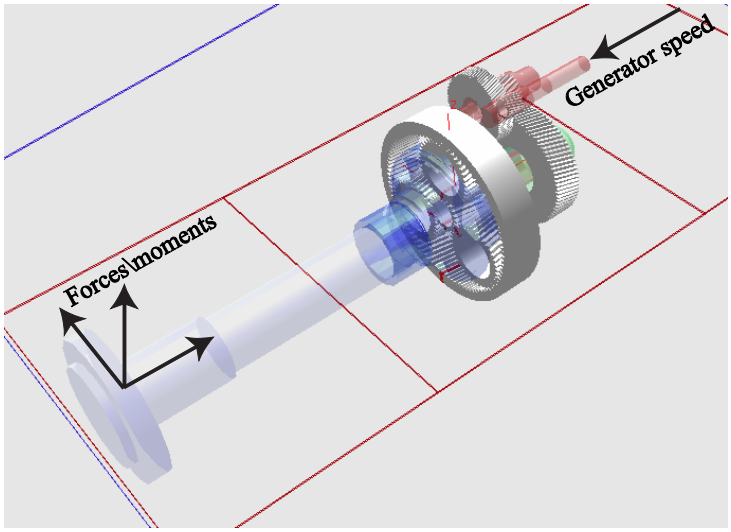

Figure 6: Application of the main-shaft loads and generator speed into the multibody drivetrain model. The torque arms and housing casings are not shown.

4. Model and Experiment Comparison

Some field-test measurements are presented in Figure 7 and Figure 8. In these figures, LSS_SPD denotes the main-shaft speed, LSS_TRQ denotes the main-shaft torque, and PL1_A and PL1_B denote the radial loads for the upwind and downwind planet gear bearings, respectively. These load cases are emergency-shutdown and start-up events. As observed, these two events caused large torque loads on the main shaft and thus large internal drivetrain loads.

Previous comparisons to the dynamometer tests focused on measurements from the low-speed planetary stage, such as the planet bearing loads, planet gear deflections, sun gear orbit, and planet carrier rim deflection. In this paper, more emphasis was placed on the responses in the higher-speed stages. This is because the loads for some of the transient events, such as emergency-brake and start-up, are applied at the generator-side of the gearbox. This means that the higher-speed stages can experience large loads, and attention was given to accurately predict these loads in the multibody model.

Unfortunately, only the planet bearing radial forces were available; measurements from the higher-speed stages were not available. The field-test measurements were sampled at 10 Hz, and similarly, the computational results were also sampled at 10 Hz for comparison purposes. Note that using a lower sampling frequency will cause some local maximum responses to go undetected.

Comparisons of the measured and predicted planet bearing forces for both the start-up and emergency-shutdown events are presented in Figure 9. The computational results were calculated using the GB04 model, which is a high-fidelity model described in Section 5.1. As seen in Figure 9, the GB04 model with 40 elastic modes for each flexible body can reproduce the planet bearing forces well. The maximum forces calculated are within 3.2% and 2.0% of the measured values for the PL1-A bearing radial forces in the emergency-brake and start-up events, respectively. This model was used as the ‘correct’ model to provide responses for comparison in the entire drivetrain for the rest of this paper. Furthermore, it was observed that the time series of the numerical results matched the measurements very well. The comparisons to the measurements showed that a multibody drivetrain model captures the transient response behaviour of the wind turbine gearbox and is certainly a useful tool for load predictions. Unfortunately, only the measurements of the loads from the planetary stage were available for comparison. Future comparisons of the responses from the higher-speed stages will need to be made for further validation of the model.

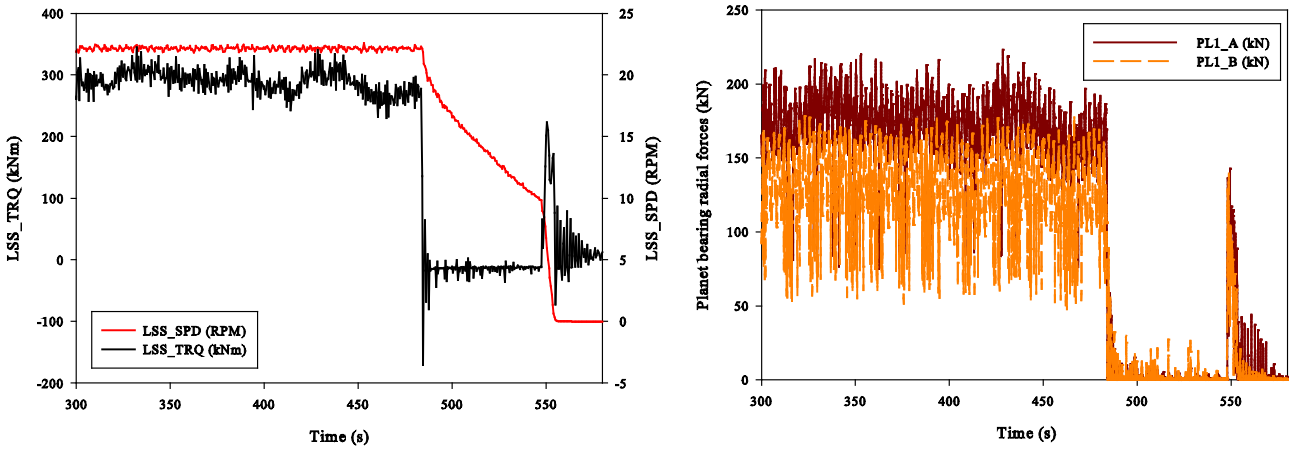

Figure 7: Emergency-shutdown event and its corresponding measured bearing loads

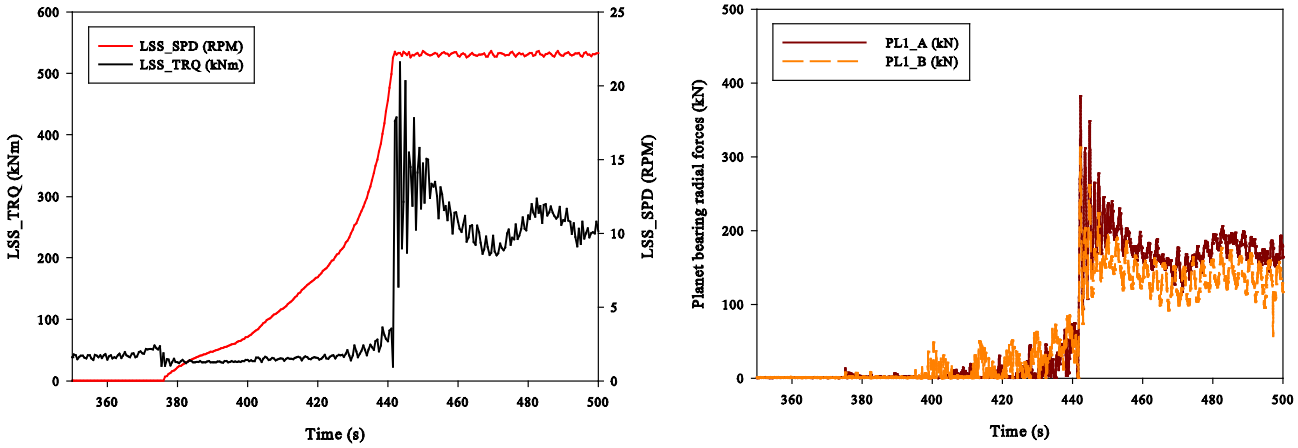

Figure 8: Start-up event and its corresponding measured bearing loads

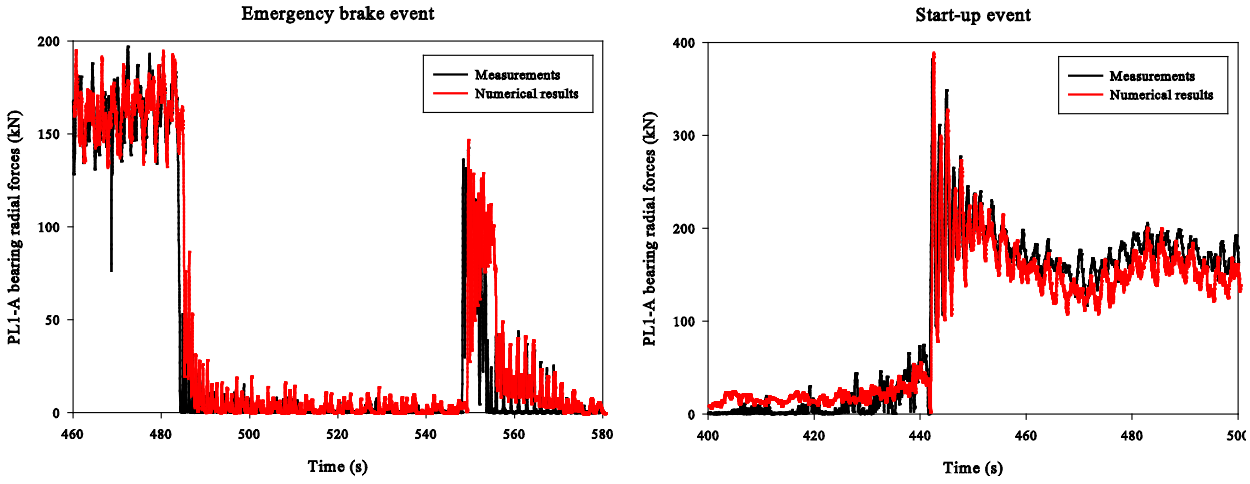

Figure 9: Comparisons of the predicted planet bearing forces against the measurement results for the start-up and emergency-shutdown events.

5. Detailed Model Study

5.1. Model Fidelity

This section describes a detailed drivetrain model fidelity study that was performed using the emergency-shutdown and start-up events as case studies. The maximum responses after the emergency brake was applied and during the start-up process were used for the comparisons.

Four different types of models were compared to the measurements in this section. The models are described as follows:

- GB00 – Fully rigid gearbox with tooth compliance and only torsional degrees of freedom
- GB01 – Fully rigid gearbox model with tooth compliance and bearing compliance
- GB02 – Addition of flexible shafts into GB01
- GB03 – Addition of flexible planet carrier into GB02
- GB04 – Addition of flexible housing and torque arms into GB03, making it a fully flexible model

The results are presented in Table 1 and Table 2. Responses that have large differences, i.e., above 20% or below minus 20%, are highlighted in yellow. The results are presented as percentage differences versus the GB04 model using the following formula:

$$\%difference = \frac{X - X_{GB04}}{X_{GB04}} \times 100\% \quad (1)$$

where X is the response variable of concern and X_{GB04} is the response variable calculated from the GB04 model. The sampling rate is 200 Hz for the comparison presented in this section, whereas in Section 4, the sampling rate was 10 Hz.

The results show that the tooth contact forces are not sensitive to the level of model detail. This means that a simplified model, i.e., GB00, can be used when only the gear contact forces are required. However, the gear contact forces here are the total integrated forces, and the load distribution along the tooth flank, i.e., face load factor, might be sensitive to the model fidelity. This was not investigated here because of the constraints of the model that was used. Future investigations into the face load factors should be conducted. On the other hand, the bearing forces at the low-, intermediate-, and high-speed shafts are sensitive to the gearbox model fidelity; the planetary stage bearings are less sensitive compared to these higher speed bearings. It was observed that the GB02 model is sufficient for the convergence of the planetary stage bearing loads. For the remaining higher-speed bearings, a GB04 model is required.

Table 1: Comparison of Important Response Variables in the Entire Drivetrain from Various Computational Models (emergency shutdown event)

	GB00	GB01	GB02	GB03
Gear contact forces				
Sun-planet	-9.38	8.14	-0.19	0.14
Intermediate speed	-1.11	-1.46	0.10	0.20
High speed	-2.51	-4.68	-0.42	-0.58
Bearing radial forces				
PL-A	-20.53	30.49	-9.06	-2.05
PL-B	-22.99	-1.11	9.45	2.11
LS-SH-B	68.02	-9.56	146.02	150.41
LS-SH-C	-22.74	-1.29	138.40	140.92
IMS-SH-B	-19.29	31.11	-5.09	-1.78
IMS-SH-C	53.88	63.39	-26.63	-26.92
HS-SH-B	276.14	-51.98	-6.32	-0.80
HS-SH-C	-10.04	47.16	17.36	9.74

Table 2: Comparison of Important Response Variables from Different Computation Models (start-up event)

	GB00	GB01	GB02	GB03
Gear contact forces				
Sun-planet	1.89	-0.10	0.66	0.50
Intermediate speed	-2.88	-0.44	-0.38	-0.33
High speed	-3.63	1.12	0.09	-0.04
Bearing radial forces				
PL-A	-17.32	-7.89	-3.46	1.61
PL-B	-4.39	4.26	8.74	0.47
LS-SH-B	60.57	-5.33	17.54	17.70
LS-SH-C	-33.97	-2.49	-1.56	-1.80
IMS-SH-B	-41.52	-14.40	2.42	2.74
IMS-SH-C	98.46	50.37	-1.08	-1.14
HS-SH-B	42.43	-73.55	77.64	78.30
HS-SH-C	-22.37	65.45	-2.34	-1.67

5.2. Flexible Modes

In this section, the flexible modes to be included in each flexible body were investigated. Each flexible mode consists of two state variables, one representing the displacement and the other representing the velocity. Using a larger number of flexible modes than required will increase the computational efforts required. The results in Section 5.1 show that the GB01 model is detailed enough for the calculation of the gear contact forces and that they did not benefit from the use of flexible bodies. Therefore, gear contact forces were not investigated in this section. The results are presented in Table 3 and Table 4 as percentage differences versus the GB04 model using Equation (1).

The following notations are used in Table 3 and Table 4:

- A10, A20 – 10, 20 elastic modes for all flexible bodies
- S10, S20 – 10, 20 elastic modes for all shafts and 40 elastic modes for the remaining flexible bodies
- S10, S20 – 10, 20 elastic modes for all shafts and 40 elastic modes for the remaining flexible bodies
- PC10, PC20 – 10, 20 elastic modes for the planet carrier and 40 elastic modes for the remaining flexible bodies
- H10, H20 – 10, 20 elastic modes for the housing and 40 elastic modes for the remaining flexible bodies
- TA10, TA20 – 10, 20 elastic modes for the torque arms and 40 elastic modes for the remaining flexible bodies

Comparing the results from Table 3 and Table 4 shows that the responses calculated under the emergency shutdown event are more sensitive to the number of modes included in the flexible bodies compared to the responses calculated under the start-up event. This suggests that the model requirements are dependent on the type of input loading to which the model is subjected. The reason for this can be explained by the differences in the nature of the main-shaft loads in each of the transient load events. In the emergency shutdown event, the maximum torque and bending moments experienced are 299.4 kNm and 168.6 kNm, respectively, while in the start-up event, the bending moments are 665.0 kNm and 195.5 kNm, respectively. The bending moments are measured at a position that is about 70% of the main shaft length from the hub connection. In the emergency shutdown event, the ratio of the bending moment to torque is 0.56, while for the start-up event it is 0.29. The higher ratio in the emergency shutdown event might demand a more flexible multibody model as the gears and shaft deflect more and therefore, are more sensitive to the prescription of the flexible bodies in the multibody model. A more thorough investigation considering more transient load events should be conducted to further validate this hypothesis.

Table 3: Comparison of Bearing Radial Forces in the Entire Drivetrain when Different Numbers of Elastic Modes are Used (emergency shutdown event)

Number of elastic modes	A10	A20	S10	S20	PC10	PC20	H10	H20	TA10	TA20
PL-A	-7.81	-5.70	-1.31	0.13	-6.61	-5.75	-0.26	-0.24	-0.23	-0.35
PL-B	7.27	5.42	0.11	-0.69	6.89	5.95	0.11	0.09	0.14	0.19
LS-SH-B	7.50	7.14	4.99	3.70	-0.22	-0.02	-0.69	-1.61	-0.12	0.20
LS-SH-C	17.16	27.85	11.95	7.82	0.58	0.43	-0.41	-1.17	0.40	0.41
IMS-SH-B	-0.14	-0.88	-1.10	-0.21	-1.28	-1.34	-1.42	-1.84	-1.41	-1.40
IMS-SH-C	17.37	11.55	-13.24	-3.68	-2.96	1.76	26.24	14.64	3.58	2.17
HS-SH-B	-51.62	-5.76	-31.69	0.91	0.09	0.07	-9.38	-8.34	1.62	0.62
HS-SH-C	35.66	-19.67	-17.08	-12.81	-0.61	-2.33	-3.06	-4.96	-10.99	-4.23

Table 4: Comparison of Bearing Radial Forces in the Entire Drivetrain when Different Numbers of Elastic Modes are Used (start-up event)

Number of elastic modes	A10	A20	S10	S20	PC10	PC20	H10	H20	TA10	TA20
PL-A	-2.31	-3.14	1.32	0.60	-4.64	-4.67	0.02	0.00	0.70	0.27
PL-B	7.10	5.34	-0.39	-0.95	7.67	6.76	-0.19	-0.29	-0.33	-0.32
LS-SH-B	5.08	0.07	4.88	-0.76	0.13	0.45	1.88	0.53	0.07	0.81
LS-SH-C	-3.90	-1.37	-2.03	-0.14	-0.30	-1.25	0.11	-0.22	0.36	-0.71
IMS-SH-B	3.61	0.65	3.57	0.49	-0.50	0.25	1.87	0.53	0.47	-0.01
IMS-SH-C	1.01	1.22	-2.56	-0.87	-0.40	-0.29	0.10	-0.68	0.13	-1.28
HS-SH-B	-2.55	7.49	-0.06	-0.45	-1.34	-1.07	-0.56	7.65	-2.46	-3.37
HS-SH-C	7.40	-6.81	9.26	-4.06	5.99	2.57	3.62	4.78	-3.68	0.11

6. Conclusions

A fully flexible model with 40 elastic modes reproduces the maximum loads experienced in the emergency shutdown and start-up events to within 3.2% and 2.0%, respectively. The time histories of calculated loads match the experiments. A fully rigid model would over predict the bearing loads by about 20%. The response variables at the higher-speed stages require a higher level of model fidelity to be represented correctly. The start-up event is not as sensitive as the emergency shutdown event to the number of modes in each flexible body. This might be because of the lower main shaft bending moment to torque ratio in the start-up event compared to the bending moment to torque ratio in the shutdown event.

Acknowledgements

This work was financially supported by the Centre for Ships and Ocean Structures (CeSOS) at the Department of Marine Technology, Norwegian University of Science and Technology, Trondheim, Norway. The gearbox and wind turbine model were obtained from the Gearbox Reliability Collaborative (GRC) project at the National Renewable Energy Laboratory, Colorado, USA. The GRC initiative is funded by the Wind and Water Power Technologies Office, Office of Energy Efficiency and Renewable Energy, the U.S. Department of Energy under contract No. DE-AC02-05CH11231.

References

[1] De Vries, E. (2006) Trouble Spots: Gearbox Failures and Design Solutions. *Renewable Energy World*, 2006, pp. 37-47.

[2] Link, H.; LaCava, W.; van Dam, J.; McNiff, B.; Sheng, S.; Wallen, R.; McDade, M.; Lambert, S.; Butterfield, S.; Oyague, F. (2011) *Gearbox Reliability Collaborative Project Report: Findings from Phase 1 and Phase 2*, National Renewable Energy Laboratory, Golden, Colorado. Report number: NREL/TP-5000-51885.

[3] LaCava, W.; Xing, Y.H.; Guo, Y.; Moan, T.; (2012). "Determining Wind Turbine Gearbox Model Complexity using Measurement Validation and Cost Comparison." European Wind Energy Association annual event, Copenhagen, 2012.

[4] LaCava, W.; Xing, Y.H.; Marks, C.; Guo, Y.; Moan, T. (2012) "Three-Dimensional Bearing Load Share Behavior in the Planetary Stage of a Wind Turbine Gearbox." Accepted, *IET Renewable Power Generation*.

[5] Xing, Y.H.; Moan, T. (2012) "Multi-Body Modelling and Analysis of a Planet Carrier in a Wind Turbine Gearbox." Accepted,*Wind Energy*.

[6] LaCava, W.; Keller, J.; McNiff, B., (2012) "Gearbox Reliability Collaborative: Test and Model Investigation of Sun Orbit and Planet Load Share in a Wind Turbine Gearbox." 53rd Structures, Structural Dynamics, and Materials and Co-located Conferences, Honolulu, Hawaii, 2012.

[7] LaCava, W.; McNiff, B.; van Dam, J. (2011). "Comparing In-Field Gearbox Response to Different Dynamometer Test Conditions - NREL Gearbox Reliability Collaborative." AWEA WINDPOWER 2011, Anaheim, CA.

[8] Oyague, F., (2009). *Gearbox Modeling and Load Simulation of a Baseline 750-kw Wind Turbine using State-of-the-Art Simulation Codes*, National Renewable Energy Laboratory, Golden, Colorado. Report number: NREL/TP-500-41160.

[9] Oyague, F. (2008). "Progressive Dynamical Drivetrain Modelling as Part of NREL Gearbox Reliability Collaborative." AWEA WINDPOWER 2008, Houston, Texas.

[10] Oyague, F.; Butterfield, C.P.; Sheng, S. (2009). "NREL Gearbox Reliability Collaborative Analysis Round Robin." American Wind Energy Association WINDPOWER 2009, Chicago, Illinois.

[11] Oyague, F.; Gorman, D.; Sheng, S. (2010). NREL Gearbox Reliability Collarborative Experimental Data Overview and Analysis." AWEA WINDPOWER 2010, Dallas, Texas.

[12] Peeters, J. (2006) *Simulation of Dynamic Drivetrain Loads in a Wind Turbine*, PhD Thesis, KU Leuven, Department of Mechanical Engineering.

[13] Peeters, J.; Vandepitte, D.; Sas, P. (2004). "Flexible Multibody Model of a Three-Stage Planetary Gearbox." International Conference on Noise and Vibration Engineering, Leuven, Belgium, 2004.

[14] Peeters, J.L.M.; Vandepitte, D.; Sas, P. (2006) "Analysis of Internal Drivetrain Dynamics in a Wind Turbine." *Wind Energy*, 2006, 9 (1-2), 141-161.

[15] Helsen, J.; Heirman, G.; Vandepitte, D.; Desmet, W. (2008). "The Influence of Flexibility within Multibody Modelling of Multimegawatt Wind Turbine Gearboxes." International Conference on Noise and Vibration Engineering, Leuven, Belgium, 2008.

[16] Helsen, J.; Vanhollebeke, F.; De Coninck, F.; Vandepitte, D.; Desmet, W. (2011) "Insights in Wind Turbine Drivetrain Dynamics Gathered by Validating Advanced Models on a Newly Developed 13.2-MW Dynamically Controlled Test-Rig." *Mechatronics*, 2011, 21 (4), 737-752.

[17] Helsen, J., Vanhollebeke, F., Marrant, B., Vandepitte, D., Desmet, W., Multibody modelling of varying complexity for modal behaviour analysis of wind turbine gearboxes, Renewable Energy 2011, 36 (11), 3098-3113.

[18] Helsen, J., Vanhollebeke, F., Vandepitte, D., Desmet, W., Optimized inclusion of flexibility in wind turbine gearbox multibody model in view of model updating on dynamic test rig, in: The 1st Joint International Conference on Multibody System Dynamics, Lapppeenranta, Finland, 2010.

[19] Xing, Y.H., Karimirad, M., Moan, T., Effect of spar-type floating wind turbine nacelle motions on drivetrain dynamics, in: European Wind Energy Association annual event, Copenhagen, 2012.

[20] Xing, Y.H., Karimirad, M., Moan, T., Modelling and analysis of floating spar-type wind turbine drivetrain, Accepted for publication in Wind Energy 2013.

[21] Guo, Y., Keller, J., LaCava, W., Combine effects of gravity, bending moment, bearing clearance, and input torque on wind turbine planetary gear load sharing, in: American Gear Manufacturers Association Fall Technical Meeting, Dearborn, Michigan, 2012.

[22] Guo, Y., Keller, J., Parker, R.G., Dynamic analysis of wind turbine planetary gears using an extended harmonic balance approach, in: International Conference on Noise and Vibration Engineering, Leuven, Belgium, 2012.

[23] ISO 6336-1: Calculation of load capacity of spur and helical gears - part 1: basic principle, introduction and general influence factors, 2006